Supplemental Methods

Mice. B6.Cg-Commd10$^{Tg(Vav1\text{-}icre)A2Kio}$/J (vav-iCre) mice[1], B6.Cg-Gt(ROSA)$^{26Sortm9(CAG\text{-}tdTomato)Hze}$/J (Rosa26-tdTomato) mice[2], B6.SJLPtprc^{a}Pepc^{b}/BoyJ (CD45.1), and C57BL/6J mice were purchased from the Jackson Laboratory and bred in house. *Gdf11*$^{+/-}$ mice[3] and Gdf11$^{fl/fl}$ mice[4] were obtained from Dr. Se-Jin Lee at the Johns Hopkins University School of Medicine (now at the Jackson Laboratory). To generate cKO, cHet, and cre- control animals, we bred and crossed *Gdf11*$^{fl/fl}$; *Rosa26*$^{tdTomato/tdTomato}$ mice to *vav*-iCre;*Gdf11*$^{fl/+}$ mice. To generate cre+ control animals (*vav*-iCre; *Rosa26*$^{tdTomato/+}$), we crossed *vav*-iCre mice to *Rosa26*$^{tdTomato/tdTomato}$ mice. To generate *Gdf11*$^{+/+}$, *Gdf11*$^{+/-}$, and *Gdf11*$^{-/-}$ embryos, timed matings of *Gdf11*$^{+/-}$ males and females were established, with detection of vaginal plug designated embryonic day 0.5 (E0.5). Primers used to PCR the *Gdf11* wt, flox, Δ, *Gdf11*$^{+}$, and *Gdf11*$^{-}$ alleles are listed in Supplemental Table 1. We used age-matched male and female mice for all analyses with no specific randomization or blinding protocols. *Gdf11*-IRES-GFP mice were generated by insertion of an IRES-GFP cassette between the last codon and the 3'UTR of *Gdf11*. This insertion produces a bicistronic transcript from the endogenous *Gdf11* locus and marks *Gdf11*-expressing cells with green fluorescence without altering the pattern or levels of endogenous *Gdf11* mRNA or protein production (J.M.G. and A.J.W., manuscript submitted June 2019).

Flow cytometry antibodies. The following antibodies were used for flow cytometry: anti-lineage cocktail-Pacific Blue (anti-CD3 (17A2), anti-CD45R/B220 (RA3-6B2), anti-CD11b (M1/70), anti-Ly-6G/Ly-6C (RB6-8C5) and anti-Ter-119 (TER-119); Biolegend, 133310, 1:20 dilution), anti-CD3-eFluor450 (145-2C11, Thermo Fisher, 48-0031-80, 1:100 dilution), anti-CD45R/B220-eFluor450 (RA3-6B2, Thermo Fisher, 48-0452-80, 1:200 dilution), anti-CD11b-eFluor450 (M1/70, Thermo Fisher, 48-0112-82, 1:800 dilution), anti-Ly-6G/Ly-6C (Gr-1)-eFluor450 (RB6-8C5, Thermo Fisher, 48-5931-82, 1:400 dilution), anti-TER-119-eFluor450 (TER-119, Thermo Fisher, 48-5921-82, 1:100 dilution), anti-Ly6A/E (Sca-1)-PE/Cy7 (D7, Biolegend, 108114, 1:200 dilution), anti-CD117 (c-Kit)-APC (2B8, BD Biosciences, 553356, 1:200 dilution), anti-CD48-FITC (HM48-1, Biolegend, 103404, 1:200 dilution), anti-CD150-BV510 (TC15-12F12.2, Biolegend, 115929, 1:50 dilution), anti-CD34-FITC (RAM34, Thermo Fisher, 11-0341-85, 1:25 dilution), anti-CD16/CD32-Alexa Fluor 700 (93, Thermo Fisher, 56-0161, 1:100 dilution), anti-CD71-FITC (C2, BD Biosciences, 553266, 1:200 dilution), anti-Ter-119-APC (TER-119, Biolegend, 116212, 1:200 dilution), anti-CD150-PE (TC15-12F12.2, Biolegend, 115904, 1:200 dilution), anti-CD41-PE (MWReg30, Biolegend, 133906, 1:200 dilution), anti-CD16/CD32 (Mouse BD FC Block) (2.4G2, BD Biosciences, 553142, 1:50 dilution), anti-CD45.1-PE (A20, Biolegend, 110708, 1:100 dilution), anti-CD45.1-PerCP (A20, Biolegend, 110726, 1:100 dilution), anti-CD45.2-APC (104, Biolegend, 109814, 1:100 dilution), anti-CD45.2-Alexa Fluor 700 (104, Biolegend, 109822, 1:100 dilution), anti-CD3-PECy/7 (17A2, Biolegend, 100220, 1:65 dilution), anti-CD45R/B220-FITC (RA3-6B2, 11-0452-85, Thermo Fisher, 1:100 dilution), anti-CD11b-APC (M1/70, Biolegend, 101212, 1:200 dilution), anti-CD11b-APC/Cy7 (M1/70, Biolegend, 101226,1:200 dilution), anti-Ly-6G-Pacific Blue (1A8, Biolegend, 127612,1:200 dilution), anti-CD3-biotin (145-2C11, Biolegend, 100309, 1:100 dilution), anti-CD45R/B220-biotin (RA3-6B2, Thermo Fisher, 13-0452-85, 1:200 dilution), anti-CD11b-biotin (M1/70, Thermo Fisher, 13-0112-85, 1:800

dilution), anti-Ly-6G/Ly-6C-biotin (RB6-8C5, Thermo Fisher, 13-5931-85, 1:400 dilution), anti-TER-119-biotin (TER-119, Biolegend, 116204, 1:100 dilution), anti-CD48-PerCP/Cy5.5 (HM48-1, Biolegend, 103421, 1:200 dilution), anti-CD71-PE (C2, BD Biosciences, 553267, 1:200 dilution), anti-CD117 (c-Kit)-PE (2B8, Biolegend, 105808, 1:200 dilution), and anti-CD34-eFluor660 (RAM34, Thermo Fisher, 50-0341-82, 1:25 dilution). 7-AAD (BD Biosciences, 559925, 1:20 dilution) or Zombie Aqua (Biolegend, 423101, 1:300 dilution) were used as viability dyes.

Flow cytometry staining and gating. To identify HSCs from *vav*-iCre; *Gdf11*; *Rosa26-tdTomato* mice and C57BL/6J transplanted recipients, bone marrow cells were stained with the following antibodies for 45 minutes on ice: Lineage cocktail-Pacific Blue, Sca-1-PE/Cy7, c-Kit-APC, CD48-FITC, and CD150-BV510. 7-AAD was added immediately prior to analysis. To identify myeloid progenitors (MPs) from *vav*-iCre; *Gdf11*; *Rosa26-tdTomato* mice, cells were stained with the following antibodies for 60 minutes on ice: Lineage cocktail-Pacific Blue, Sca-1-PE/Cy7, c-Kit-APC, CD34-FITC, CD16/CD32-Alexa Fluor 700 and Zombie Aqua. To identify erythroid precursor cells from *vav*-iCre; *Gdf11*; *Rosa26-tdTomato* mice, cells were stained with the following antibodies for 30 minutes on ice: Ter119-APC and CD71-FITC, and 7-AAD was added immediately prior to flow analysis. To assess donor chimerism in C57BL/6J transplanted recipients, peripheral blood cells were blocked with anti-CD16/CD32 for 5 minutes on ice, following by incubation with the following antibodies for 30 minutes on ice: CD3-PE/Cy7, B220-FITC, CD11b-APC and Ly-6G-Pacific Blue, and 7-AAD was added prior to analysis.

To identify HSCs from fetal livers, cells were stained with the following antibodies/dyes for 45 minutes on ice: Lineage cocktail-Pacific Blue, Sca-1-PE/Cy7, c-Kit-APC, CD48-FITC, CD150-PE, and Zombie Aqua. To identify EPCs from fetal livers, cells were stained with the following antibodies/dyes for 30 minutes on ice: CD3-eFluor450, B220-eFluor450, CD11b-eFluor450, Gr-1-eFluor450, CD41-PE, CD71-FITC, Ter-119-APC, and Zombie Aqua. Fetal liver cells were fixed in 1% paraformaldehyde prior to analysis. To assess donor chimerism in CD45.1 transplanted recipients, peripheral blood cells were blocked with anti-CD16/CD32 for 5 minutes on ice, following by incubation with the following antibodies/dyes for 30 minutes on ice: CD3-PE/Cy7, B220-FITC, CD11b-APC/Cy7 and Ly-6G-Pacific Blue, CD45.1-PE, CD45.2-APC, and Zombie Aqua. To identify HSCs from CD45.1 transplanted recipients, cells were stained with the following antibodies/dyes for 45 minutes on ice: Lineage cocktail-Pacific Blue, Sca-1-PE/Cy7, c-Kit-APC, CD48-FITC, CD150-PE, CD45.1-PerCP, CD45.2-Alexa Fluor 700, and Zombie Aqua.

To identify HSCs from *Gdf11*-GFP mice, cells were stained with the following antibodies/dyes for 45 minutes on ice: Lineage cocktail-Pacific Blue, Sca-1-PE/Cy7, c-Kit-APC, CD48-FITC, CD150-PE, and Zombie Aqua. To identify EPCs from *Gdf11*-GFP mice, cells were stained with the following antibodies/dyes for 30 minutes on ice: CD71-PE, Ter-119-APC, and Zombie Aqua. To identify MPs from *Gdf11*-GFP mice, cells were stained with the following antibodies/dyes for 60 minutes on ice: Lineage cocktail-Pacific Blue, Sca-1-PE/Cy7, c-Kit-PE, CD34-APC, CD16/CD32-Alexa Fluor 700, and Zombie Aqua.

HSCs were gated as Lineage$^-$Sca-1$^+$-c-Kit$^+$CD48$^-$CD150$^+$. MPs were gated as Lineage$^-$ Sca-1$^-$c-Kit$^+$, and subsequently gated to identify common myeloid progenitors (CMPs; CD34$^+$CD16/CD32^{low}), granulocyte-monocyte progenitors (GMPs; CD34$^+$CD16/CD32$^+$), and megakaryocyte-erythrocyte progenitors (MEPs; CD34$^-$CD16/CD32$^-$). EPCs were gated as Ter-119$^+$ cells, and subsequently gated to identify EryA (CD71^{high}FSC^{high}), EryB (CD71^{high}FSC^{low}), and EryC (CD71^{low}FSC^{low}) cells. For EPCs from fetal liver samples, cells were gated as Lineage$^-$CD41$^-$ prior to gating on Ter-119$^+$ cells. Fetal liver EPC subsets were identified as S1 (CD71^{high}Ter-119^{low}), S2 (CD71^{high}Ter-119^{mid}), S3 (CD71^{high}Ter-119^{high}), S4 (CD71^{mid}Ter-119^{high}), or S5 (CD71^{low}Ter-119^{high}).

RNA isolation. For *Gdf11*$^{+/+}$, *Gdf11*$^{+/-}$, and *Gdf11*$^{-/-}$ embryos, fetal livers were isolated and snap frozen in liquid nitrogen. For cKO, cHet, cre+ control, and cre- control animals, spleens were snap frozen in liquid nitrogen. Tissues were homogenized in Trizol (Thermo Fisher) and the aqueous phase was collected according to the manufacturer's protocol. The aqueous phase was mixed with an equal volume of 70% ethanol, purified using the RNeasy mini kit (Qiagen), and RNA concentration was calculated using a NanoDrop (Thermo Fisher).

cDNA synthesis and Real-time PCR. RNA was reverse transcribed using the SuperScript III First-Strand Synthesis Supermix (Thermo Fisher). Real-time PCR analysis was performed using RT2 SYBR Green ROX FAST master mix (Qiagen) on an ABI 7900HT sequence detection system. No reverse transcriptase (RT) controls were performed to control for the presence of genomic DNA. Real-time PCR primers are listed in Supplemental Table 1.

3' Rapid Amplification of cDNA ends (RACE). First strand cDNA synthesis was performed from 5μg total RNA using the 3' RACE system for Rapid Amplification of cDNA Ends (Thermo Fisher) according to the manufacturer's protocol. Amplification of the target cDNA was performed using a *Gdf11* gene specific primer and the abridged universal amplification primer (AUAP). Further amplification was performed using a *Gdf11* nested gene specific primer the universal amplification primer (UAP). Primer sequences are listed in Supplemental Table 1. The amplicon was gel purified using the QiaQuick Gel Extraction Kit (Qiagen), cloned using the Zero Blunt TOPO PCR Cloning kit (Thermo Fisher), transformed into Top10 Chemically Competent *E. Coli*, and sequenced by bacterial colony sequencing using the T7 and M13R primers (Genewiz).

Analysis of transcriptional adaptation. To investigate whether transcriptional adaptation[5,6] might occur in mice carrying the *Gdf11*$^-$ or *Gdf11*Δ alleles, we first identified sequence-similar genes to the wild-type *Gdf11* gene using BLASTn analysis and profiled expression of these genes. The BLASTn analysis identified six sequence-similar genes: *Bmp6, Bmp7, Fam43a, Gdf7, Inhbb,* and *Mstn*. No differences in expression of these genes were observed among cohorts containing the *Gdf11*$^-$ allele (Supplemental Figure 5a-f) or the *Gdf11*Δ allele (Supplemental Figure 6a-f). We next analyzed the mRNA transcript produced by the mutant alleles using 3' RACE and profiled expression of genes similar in sequence to the mutant transcript. We were unable to detect an mRNA transcript from the *Gdf11*$^-$ allele by 3'RACE from E14.5 *Gdf11*$^-$ FL cells (data not shown). We did

detect an mRNA transcript from the *Gdf11*Δ allele in whole spleen from 8-11 month old cKO mice (Supplemental Figure 6g). We identified six sequence-similar genes to this transcript using BLASTn: *Agtrap*, *C5ar2, Cd300a, Dcun1d2, Fasn,* and *Slc16a6*. Expression of these six genes in spleen tissue from a cohort of 8-11 month old cKO, cHet, cre+ control, and cre- control mice showed no significant differences based on genotype (Supplemental Figure 6h-m). Collectively, these findings suggest that genetic compensation through transcriptional adaptation is not occurring in our *Gdf11* loss-of-function models. Whether the effects of *Gdf11* loss may be mitigated by another, as yet unknown and redundant pathway, remains to be determined.

Supplemental Text

Rationale for evaluating the impact on blood formation and age-related phenotypes of loss of *Gdf11* within the hematopoietic compartment. Clinical studies using the ActRIIA ligand trap ACE-011 (also known as sotatercept) to treat postmenopausal women with bone loss have revealed unexpected increases in red blood cell (RBC) counts, hematocrit, and hemoglobin levels[7], suggesting that ActRII ligand inhibition might be effective in treating anemia. In addition, administration of ActRII ligand traps in several rodent models of anemia produced increases in RBC counts and hemoglobin levels, along with improved maturation of late-stage EPCs[8,9]. Outside of a disease context, treatment with the ActRIIB ligand trap ACE-536 has been reported to increase RBC counts, hematocrit and hemoglobin levels in multiple species, and both RAP-011 and ACE-536 treatment boosted the frequency of EPC populations[8,9]. Together, these data are consistent with a role for ActRII ligands in restraining both normal and stress-associated erythropoiesis.

Yet, while both the ActRIIA and ActRIIB ligand traps inhibit multiple ligands of the activin subclass (including Activin A, Activin B, GDF8 and GDF11), two of the reports cited above[8,9] concluded that the improvements in erythropoiesis induced by these chimeric receptors occurred particularly due to inhibition of GDF11. These studies proposed a model in which GDF11 promotes the survival and accumulation of immature EPCs and blocks their differentiation via an autocrine feedback loop[10]. However, this model was not tested genetically to distinguish the specific importance of particular ActRII ligands, and potential effects on formation and function of other blood lineages or in HSPC biology have not been explored.

Circulating ActRII ligands have also been studied in the context of aging, with multiple studies associating changes in circulating GDF11 in particular with the emergence, progression or reversal age-related cardiac hypertrophy and skeletal muscle dysfunction[11-13]. The enriched expression of *Gdf11* in the spleens of young animals[12,14] additionally raises the possibility that hematopoietic cells might serve as a cellular source for circulating GDF11 protein *in vivo*, and that manipulation of hematopoietic expression of *Gdf11* during youth might influence the timing of onset of certain aging phenotypes. This work, while still somewhat controversial[15,16], suggests a potential role for GDF11 produced by blood cells in the normal physiological process of aging, which similarly has yet to be tested genetically.

Motivated by these observations, in this study we utilized two independent mouse genetic models to test whether GDF11 production by hematopoietic-lineage cells indeed regulates erythropoiesis and influences cardiac size. We further explored the impact of genetic deletion of *Gdf11* on the frequency and function of HSPCs, both in steady-state conditions and following myeloablative transplant, and tested the hypothesis that hematopoietic cells may contribute to the circulating pool of GDF11.

Importance of including cre+ and cre- controls. In this study, we evaluated whether loss of hematopoietic-derived *Gdf11* might alter cardiac or skeletal muscle mass. In most of our analyses, we found that mice harboring *Gdf11*-deleted hematopoietic cells showed no changes in cardiac or skeletal muscle mass. However, in the 7-10 month old cohort, but not the 2-4 month old cohort, cHet and cKO females exhibited increased heart size relative to only the cre+ control group, but not to the cre- control group (Supplemental Figure 10r). We similarly detected significant differences in HSPC frequency relative to only one, but not both, control groups (Figure 2d-f). We conclude from these results that the observed phenotypes cannot be attributed to *vav*-lineage-specific deletion of *Gdf11*. These observations underscore the importance of including both cre+ and cre- control groups in cre/lox genetic studies, as comparison to both genotypes is essential to control for possible effects of the floxed alleles or Cre transgene on the observed phenotypes, which have been noted in prior studies from our group and others[17-19].

Contributions to the circulating pool of GDF11 protein. Given that hematopoietic cells express high levels of *Gdf11* mRNA in young animals[12], it was reasonable to hypothesize that hematopoietic cells might be a major producer of GDF11 in circulation and that deleting *Gdf11* in the hematopoietic lineage would lead to decreased serum GDF11 levels. Our quantification of GDF11 protein levels in serum, using a direct LC-MS/MS assay that does not depend on immunocapture-based enrichment, revealed that serum GDF11 does decline in the *vav*-lineage *Gdf11* knockout mouse model relative to controls (Supplemental Figure 4k). These results suggest that *vav*-expressing cell types do contribute to the overall pool of GDF11 protein in circulation during homeostasis. However, analysis of GDF11 serum levels in recipient animals transplanted with $Gdf11^{-/-}$ FL cells did not reveal significant changes when compared with recipients of $Gdf11^{+/+}$ FL cells (Supplemental Figure 2k). One key difference between these two models is that the transplanted recipients of $Gdf11^{-/-}$ FL cells had been lethally irradiated prior to transplantation, and it is unclear how total body irradiation might influence the production and/or stability of GDF11 protein in circulation. Thus, while hematopoietic cells may be significant contributors to circulating GDF11 in the steady-state, they may contribute much less to blood-borne GDF11 levels after transplant. It is also possible that, if the *vav*-iCre allele deletes in a portion of non-hematopoietic cells[20,21] or in poorly transplantable hematopoietic lineages like microglia or Langerhans cells, then the removal of *Gdf11* from these additional cell types in the *vav*-iCre model may underlie the significant decreases in serum GDF11 levels seen in the cKO and cHet mice but not in the $Gdf11^{-/-}$ FL chimeras (which lack *Gdf11* only in reconstituted hematopoietic cells). Additional conditional deletion models will help to tease apart the major contributors of GDF11 in the serum.

Supplemental Tables

Supplemental Table 1. Primer sequences.

Primer Name	Sequence (5'-3')	Purpose
*Gdf11*_a	ATGCAGATGGTAATACTTGGG	PCR of *Gdf11* wt, flox and Δ alleles
*Gdf11*_b	AAGGCTTGGGAAGCAGGCAAG	PCR of *Gdf11* wt, flox and Δ alleles
*Gdf11*_c	AGGTATGGTTAGGGTGTGGAG	PCR of *Gdf11* wt, flox and Δ alleles
*Gdf11*_F	CTACCACCGAGACGGTCATAA	Real-time PCR
*Gdf11*_R	CCGAAGGTACACCCACAGTT	Real-time PCR
*Hprt*_F	TCAGTCAACGGGGGACATAAA	Real-time PCR
*Hprt*_R	GGGGCTGTACTGCTTAACCAG	Real-time PCR
*Bmp6*_F	AGAAGCGGGAGATGCAAAAGG	Real-time PCR
*Bmp6*_R	GACAGGGCGTTGTAGAGATCC	Real-time PCR
*Bmp7*_F	ACCCCTACAAGGCCGTCTT	Real-time PCR
*Bmp7*_R	GATGGTGGTATCGAGGGTGGA	Real-time PCR
*Fam43a*_F	CCATGCAGTTGGAATGTGAGG	Real-time PCR
*Fam43a*_R	CCCAGGTCACTAATAAGCTGTG	Real-time PCR
*Gdf7*_F	GAGGGCGTTTGCGACTTTC	Real-time PCR
*Gdf7*_R	CTGCTTGTAGACCACGTTGTT	Real-time PCR
*Inhbb*_F	AACTGCTCCCCTATGTCCTGG	Real-time PCR
*Inhbb*_R	CCGCTACGTTTCAGGTCCAC	Real-time PCR
*Mstn*_F	CAGCCTGAATCCAACTTAGGC	Real-time PCR
*Mstn*_R	ACCTCTTGGGTGTGTCTGTCA	Real-time PCR
*Agtrap*_F	ATGCTTGGGGCAACTTCACTA	Real-time PCR
*Agtrap*_R	GCAGCAAGAGAAGGGCTTCA	Real-time PCR
*C5ar2*_F	GGAGACCTCTTCCTACTGGCTT	Real-time PCR
*C5ar2*_R	AGCCTACGGTAGACAGCAGAAG	Real-time PCR
*Cd300a*_F	TCAAAGCTGATAGGCATCCAGA	Real-time PCR
*Cd300a*_R	CTGCAAATTCACATACTGGCAC	Real-time PCR
*Dcun1d2*_F	GAGGCGTTTCACCGAGAGTC	Real-time PCR
*Dcun1d2*_R	TGGGTCTTTGTACCTGCTGTA	Real-time PCR
*Fasn*_F	GGAGGTGGTGATAGCCGGTAT	Real-time PCR
*Fasn*_R	TGGGTAATCCATAGAGCCCAG	Real-time PCR
*Slc16a6*_F	AGGGGTAATCTCGGGTTTAGG	Real-time PCR
*Slc16a6*_R	CCGAACGCCTTTTGTCAAAGT	Real-time PCR
*β-actin*_F	ATCAAGATCATTGCTCCTCCTGAG	Real-time PCR
*β-actin*_R	CTGCTTGCTGATCCACATCTG	Real-time PCR

*Gdf11*KO_F	GGATCGGCCATTGAACAAGATG	Embryo genotyping
*Gdf11*KO_R	GAGCAAGGTGAGATGACAGGAG	Embryo genotyping
*Gdf11*WT_F	GAGTCCCGCTGCTGCCGATATCC	Embryo genotyping
*Gdf11*WT_R	TAGAGCATGTTGATTGGGGACAT	Embryo genotyping
*Sry*_F	TTGTCTAGAGAGCATGGAGGGCCATGTCAA	Embryo genotyping
*Sry*_R	CCACTCCTCTGTGACACTTTAGCCCTCCGA	Embryo genotyping
*Gdf11*_gene specific primer	CTGCGCCTAGAGAGCATCAAG	3'RACE Target DNA Amplification
AUAP	GGCCACGCGTCGACTAGTAC	3'RACE Target DNA Amplification
*Gdf11*_nested gene specific primer	GGGAGGTAGTGAAGCAGCTG	3'RACE Target DNA Amplification Nested PCR
UAP	CUACUACUACUAGGCCACGCGTCGACTAGTAC	3'RACE Target DNA Amplification Nested PCR

Supplemental Figures

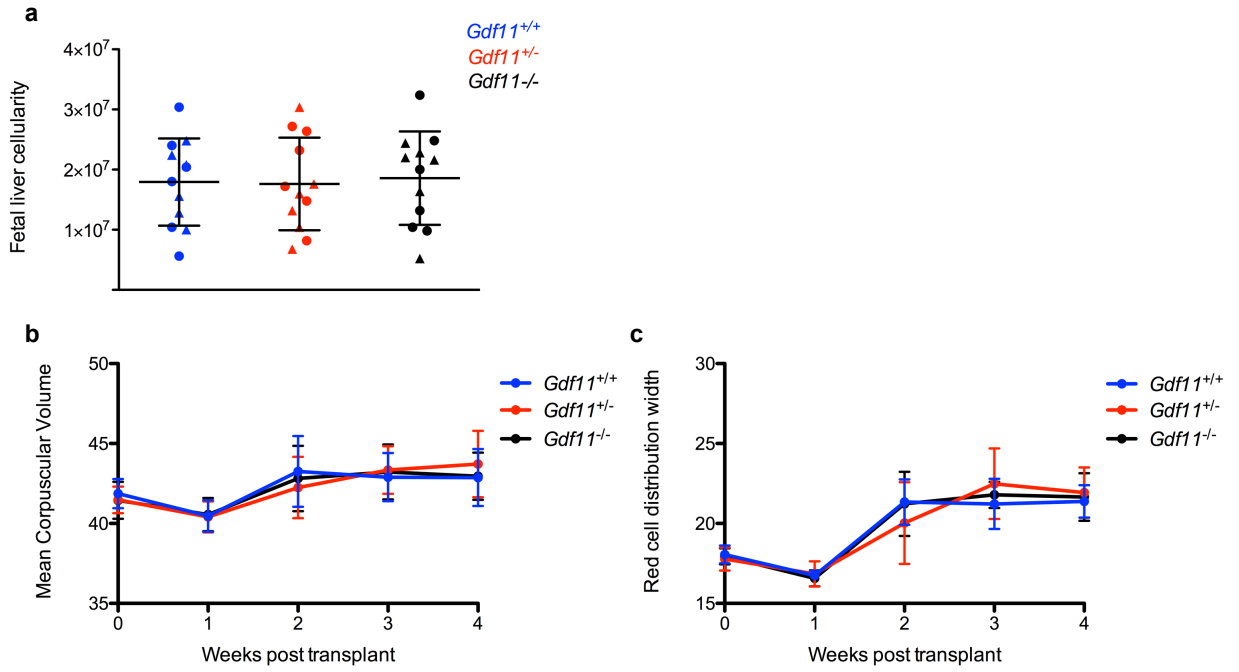

Supplemental Figure 1. Whole-body *Gdf11* deletion does not alter fetal liver cellularity during homeostasis or affect red blood cell recovery following fetal liver transplantation. (a), Quantification of fetal liver cellularity in E14.5 embryos (n=6 male and 6 female embryos per genotype). Individual data points are overlaid with mean ± SD. Statistics were calculated using a one-way ANOVA with Bonferroni post-test correction. No differences with $p<0.05$ were detected. Circles: males. Triangles: females. (b-c), (b) Mean corpuscular volume and (c) red cell distribution width in CD45.1 recipient mice transplanted with *Gdf11*$^{+/+}$, *Gdf11*$^{+/-}$ or *Gdf11*$^{-/-}$ fetal liver cells. Recipients were analyzed at 0, 1, 2, 3 and 4 weeks post-transplant (n=20 recipients per donor genotype; males and females pooled). Data are mean ± SD. Statistics were calculated using a repeated measures ANOVA, and no differences with $p<0.05$ were detected.

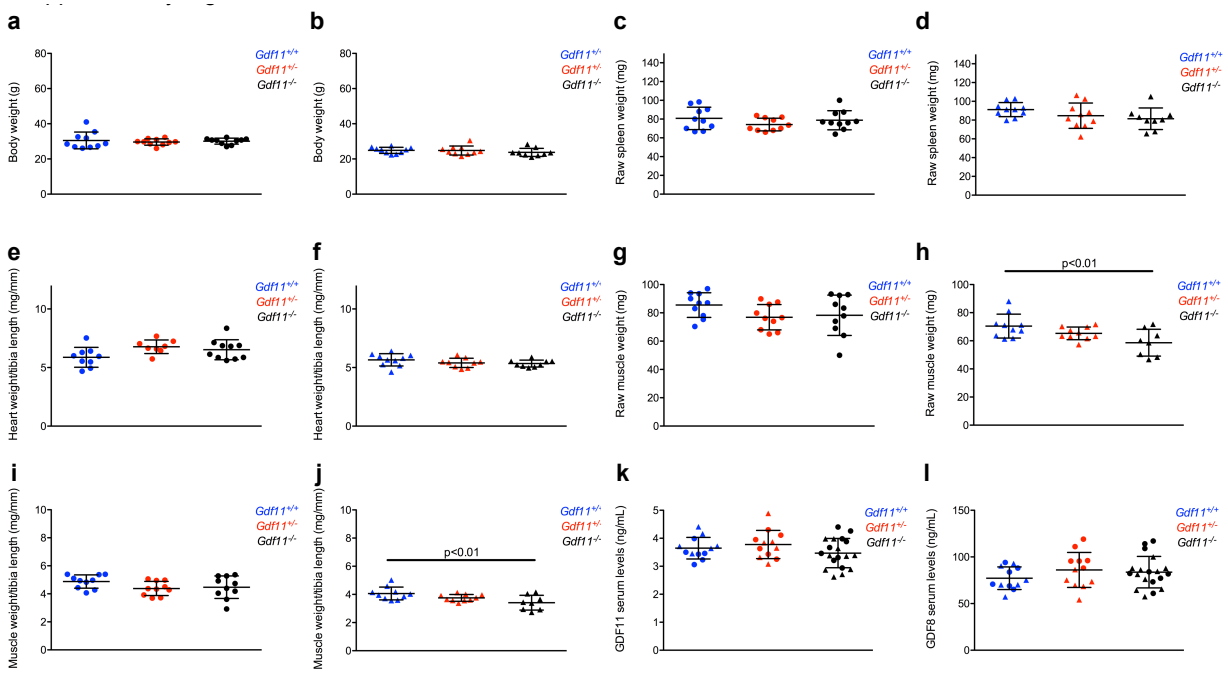

Supplemental Figure 2. Whole-body *Gdf11* deletion leads to reduced skeletal muscle mass in female mice following fetal liver transplantation. (a-b), Body weight, (c-d), raw spleen weight, (e-f), heart weight/tibia length ratio, (g-h), raw tibialis anterior muscle weight, and (i-j), tibialis anterior muscle weight/tibia length ratio in CD45.1 recipient mice at 6-7 months post-transplant (n=8-10 recipients per sex per donor genotype). (k-l), Quantification of GDF11 and GDF8 proteins in serum in CD45.1 recipient mice at 4-5 months post-transplant (n=8-10 recipients per sex per donor genotype). Individual data points are overlaid with mean ± SD. Statistics were calculated using a one-way ANOVA with Bonferroni post-test correction, and differences with $p<0.05$ are indicated. Circles: males. Triangles: females.

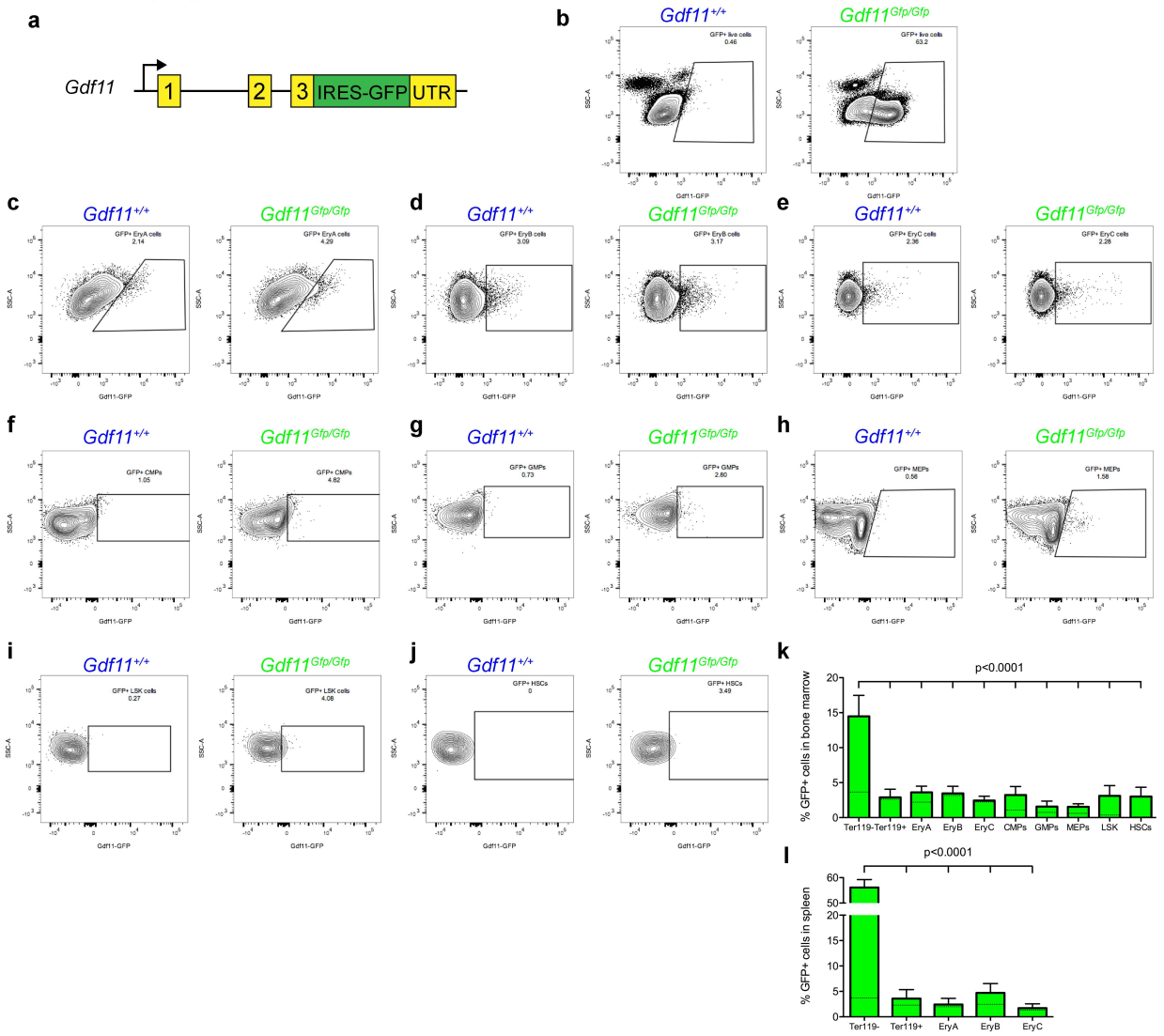

Supplemental Figure 3. *Gdf11* is minimally expressed by hematopoietic stem and progenitor cells. (a), Schematic of *Gdf11*-IRES-GFP knock-in reporter allele. (b), Representative flow cytometry analysis of GFP expression within live peripheral blood cells from 2-4 month old WT (*Gdf11*$^{+/+}$) or *Gdf11*-GFP homozygous (*Gdf11*$^{Gfp/Gfp}$) mice. (c-e), Representative flow cytometry analysis of GFP expression within bone marrow (c) EryA, (d) EryB, and (e) EryC erythroid precursor cells from 2-4 month old *Gdf11*$^{+/+}$ or *Gdf11*$^{Gfp/Gfp}$ mice. (f-h), Representative flow cytometry analysis of GFP expression within bone marrow (f) CMPs, (g) GMPs, and (h) MEPs from 2-4 month old *Gdf11*$^{+/+}$ and *Gdf11*$^{Gfp/Gfp}$ mice. (i-j), Representative flow cytometry analysis of GFP expression within bone marrow (i) Lineage^{-}Sca-1^{+}c-Kit^{+} (LSK) cells, and (j) Lineage^{-}Sca-1^{+}c-Kit^{+}CD48^{-} CD150^{+}HSCs from 2-4 month old *Gdf11*$^{+/+}$ and *Gdf11*$^{Gfp/Gfp}$ mice. (k-l), Quantification of the frequency of GFP+ cells among hematopoietic stem and progenitor cell subsets in (k) bone marrow or (l) spleen (n=6-8 mice; males and females pooled). Data are mean ± SD. Dotted lines on each bar denotes percentage of cells in GFP+ gate from the equivalent cell subset in *Gdf11*$^{+/+}$ WT controls. Statistics were calculated using one-way ANOVA with Bonferroni post-test correction, and differences with $p<0.05$ are indicated.

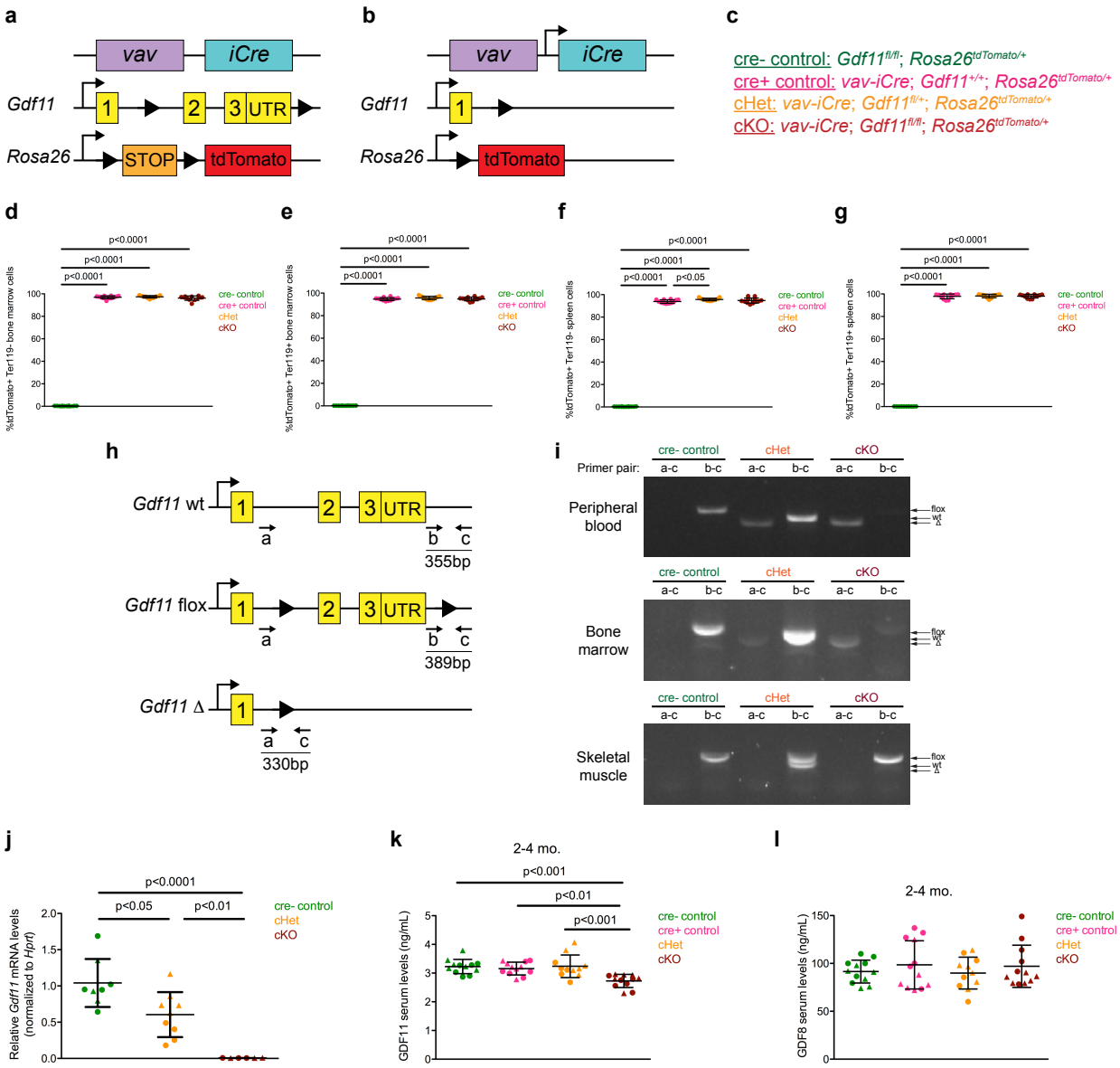

Supplemental Figure 4. Validation of the hematopoietic-specific *Gdf11* deletion mouse model. (a-b), Genetic strategy to selectively delete *Gdf11* and induce tdTomato expression within *vav*-lineage cells while keeping *Gdf11* expression intact within non-*vav*-lineage cells. Schematics depict each of the three alleles [*vav*-iCre (top), *Gdf11*^{fl} (middle), and *Rosa26*^{tdTomato} (bottom)] in the configuration expected for (a) non-hematopoietic, and (b) hematopoietic lineage cells. This strategy enables *vav*-lineage specific deletion of *Gdf11* together with irreversible induction of tdTomato fluorescence to mark Cre-expressing cells and their progeny. The *vav* promoter elements drive gene expression in a portion of FL hematopoietic cells beginning at E12.5 and are active in nearly all major hematopoietic lineages postnatally, including hematopoietic progenitor cells[22]. The *vav*-iCre transgene has also been reported to be active in the testes[1] and a subset of endothelial cells[20], although a recent study reported no detectable *vav*-iCre-mediated gene recombination within BM vascular endothelial cells[21]. *vav*-iCre activity also was reported in a subset (~30%) of bone cells with unknown identity (Lin$^-$CD45$^-$CD31$^-$CD51$^-$

Sca-1$^-$) that lack hematopoietic markers[21]. (c), Mouse genotypes and nomenclature used for experimental analyses. (d-g), Frequency of tdTomato+ cells among (d) Ter-119$^-$ bone marrow cells, (e) Ter-119$^+$ bone marrow cells, (f) Ter-119$^-$ spleen cells, and (g) Ter-119$^+$ spleen cells in mice of the indicated genotypes. In all groups containing the *vav*-iCre transgene, tdTomato fluorescence was detected within nearly all Ter-119$^-$ and Ter-119$^+$ cells in the BM and spleen, indicating robust cre activity within the hematopoietic lineage. (h), Schematic of *Gdf11* wt (top), *Gdf11* flox (middle), and *Gdf11*Δ (bottom) alleles. a, b, and c denote primer binding sites with amplicon sizes listed below. (i), Genomic DNA PCR for *Gdf11* wt (b-c amplicon: 355bp), *Gdf11* flox (b-c amplicon: 389bp), and *Gdf11*Δ (a-c amplicon: 330bp) amplicons in peripheral blood (top), bone marrow (middle), and quadriceps skeletal muscle (bottom) from a representative cKO, Het, and cre- control mouse. These data confirm recombination of the *Gdf11* floxed allele (assessed by amplification of the *Gdf11*Δ product) in the BM and spleen of cKO and cHet mice, but not in cre- controls. (j), Real time PCR analysis of *Gdf11* expression in splenocytes isolated from cKO, Het, and cre- control mice. *Hprt* was used as a housekeeping gene. Relative mRNA levels for all samples are normalized to the cre- control group. (k-l), Concentration of (k) GDF11 and (l) GDF8 protein in serum in cKO, Het, cre- control, and cre+ control mice at 2-4 months old (n=10-12 mice per genotype; males and females pooled). Individual data points are overlaid with mean ± SD. Statistics were calculated using one-way ANOVA with Bonferroni post-test correction, and differences with $p<0.05$ are indicated. Circles: males. Triangles: females.

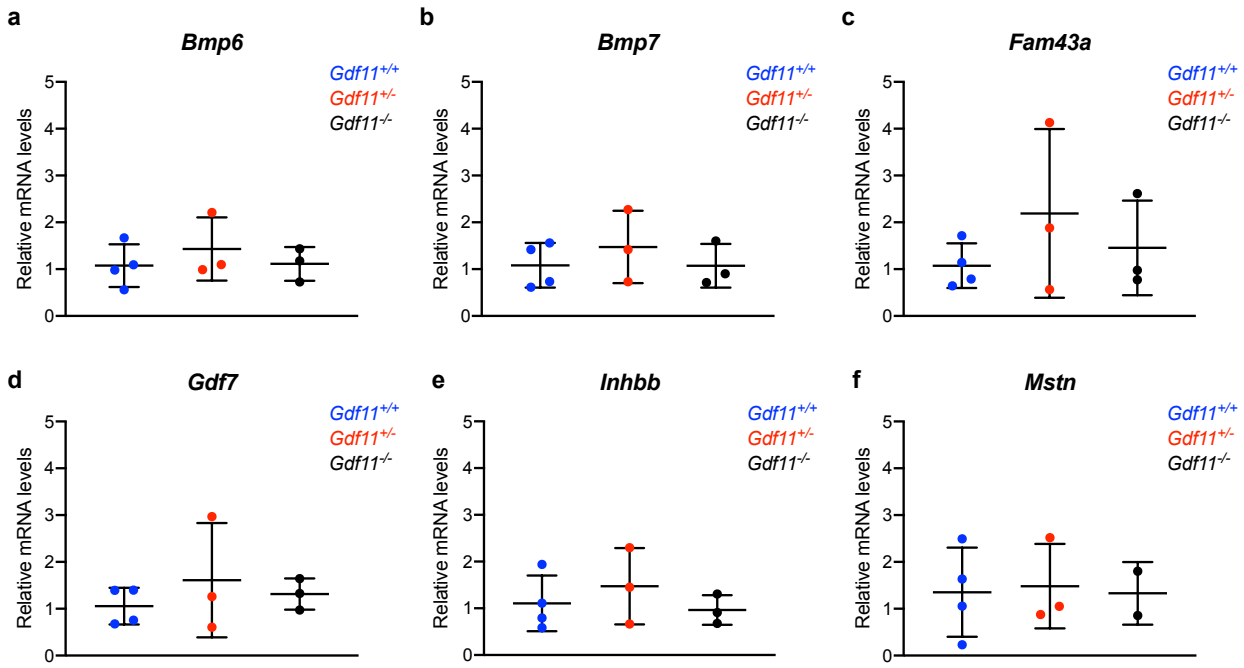

Supplemental Figure 5. Lack of transcriptional adaptation in *Gdf11*$^{-/-}$ fetal livers. Two recent reports[5,6] detailed a mechanism of genetic compensation known as transcriptional adaptation, which occurs when mRNAs produced from genes containing premature stop codons undergo nonsense mediated decay and upregulate sequence-similar genes occurs. To explore whether transcriptional adaptation might occur in embryos containing the *Gdf11*$^{-}$ allele, we profiled the expression levels of sequence-similar genes to the wild-type *Gdf11* mRNA transcript (see Supplemental Methods). (a-f), Real-time PCR analysis of (a) *Bmp6*, (b) *Bmp7*, (c), *Fam43a*, (d) *Gdf7*, (e) *Inhbb*, and (f) *Mstn* mRNA expression levels in fetal livers from E14.5 *Gdf11*$^{+/+}$, *Gdf11*$^{+/-}$, *and Gdf11*$^{-/-}$ embryos (n=3 embryos per genotype). Relative mRNA levels were calculated using β-*actin* as a housekeeping gene. Individual data points are overlaid with mean ± SD. Statistics were calculated using a one-way ANOVA with Bonferroni post-test correction. No differences with $p<0.05$ were detected. Circles: males.

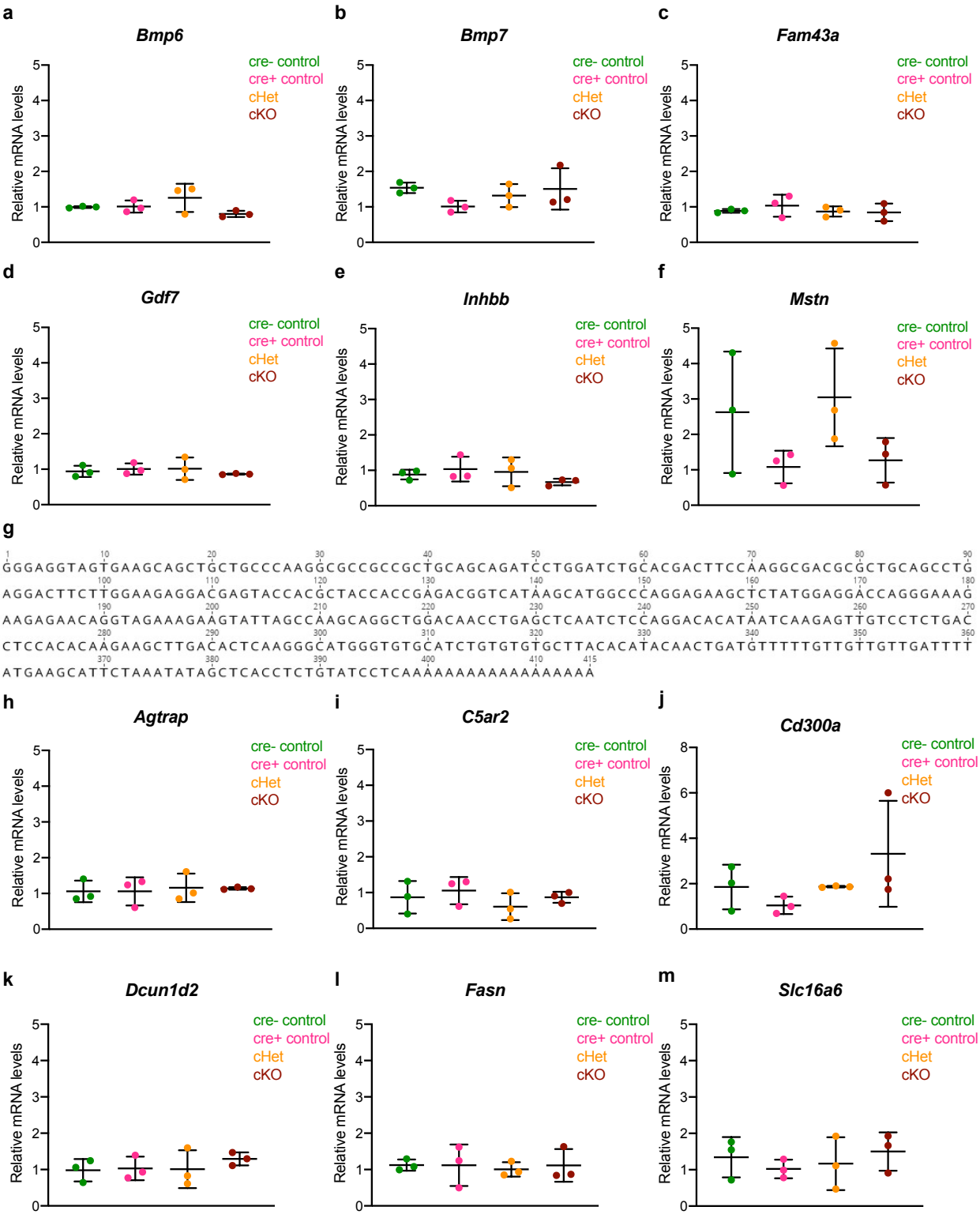

Supplemental Figure 6. Lack of transcriptional adaptation in hematopoietic-specific *Gdf11* deleted cells. To assess possible transcriptional adaptation[5,6] in mice containing the *Gdf11*Δ allele, we profiled expression levels of sequence-similar genes to the wild-type *Gdf11* mRNA transcript and the mRNA transcript produced by the *Gdf11*Δ

gene (see Supplemental Methods). (a-f), Real-time PCR analysis of (a) *Bmp6*, (b) *Bmp7*, (c), *Fam43a*, (d) *Gdf7*, (e) *Inhbb*, and (f) *Mstn* mRNA expression levels in spleen from 8-11 month old cKO, cHet, cre+ control, and cre- control mice (n=3 mice per genotype). Relative mRNA levels were calculated using *β-actin* as a housekeeping gene. (g) Consensus sequence of the mRNA transcript from the *Gdf11* Δ allele as determined by 3'RACE. (h-m), Real-time PCR analysis of (h) *Agtrap*, (i) *C5ar2*, (j), *Cd300a*, (k) *Dcun1d2*, (l) *Fasn*, and (m) *Slc16a6* mRNA expression levels in spleen from 8-11 month old cKO, cHet, cre+ control, and cre- control mice (n=3 mice per genotype). Individual data points are overlaid with mean ± SD. Statistics were calculated using a one-way ANOVA with Bonferroni post-test correction, and no differences with $p<0.05$ were detected. Circles: males.

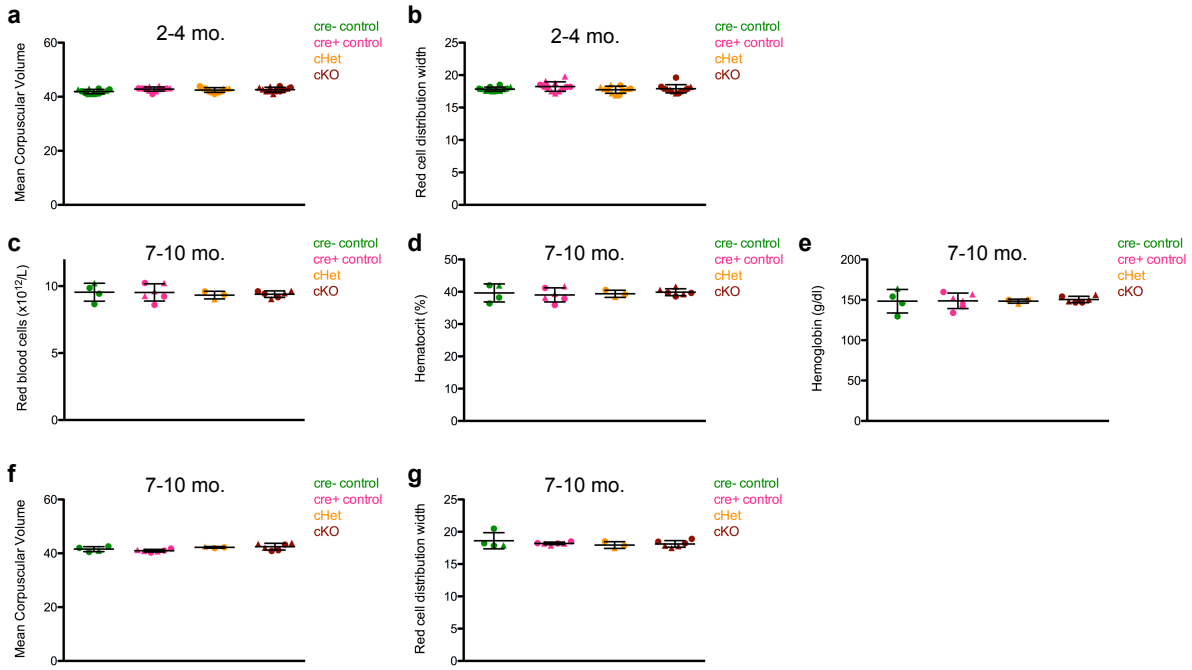

Supplemental Figure 7. *Gdf11* deletion within hematopoietic lineage cells does not alter red blood cell parameters during young adulthood or middle age. (a), Mean corpuscular volume and (b), red cell distribution width in 2-4 month old mice (n=5-6 mice per sex per genotype). (c), Red blood cell counts, (d), hematocrit, (e), hemoglobin, (f), mean corpuscular volume, and (g), red cell distribution width in 7-10 month old mice (n=3-6 mice per genotype; males and females pooled). Individual data points are overlaid with mean ± SD. Statistics were calculated using one-way ANOVA with Bonferroni post-test correction. No differences with $p<0.05$ were detected. Circles: males. Triangles: females.

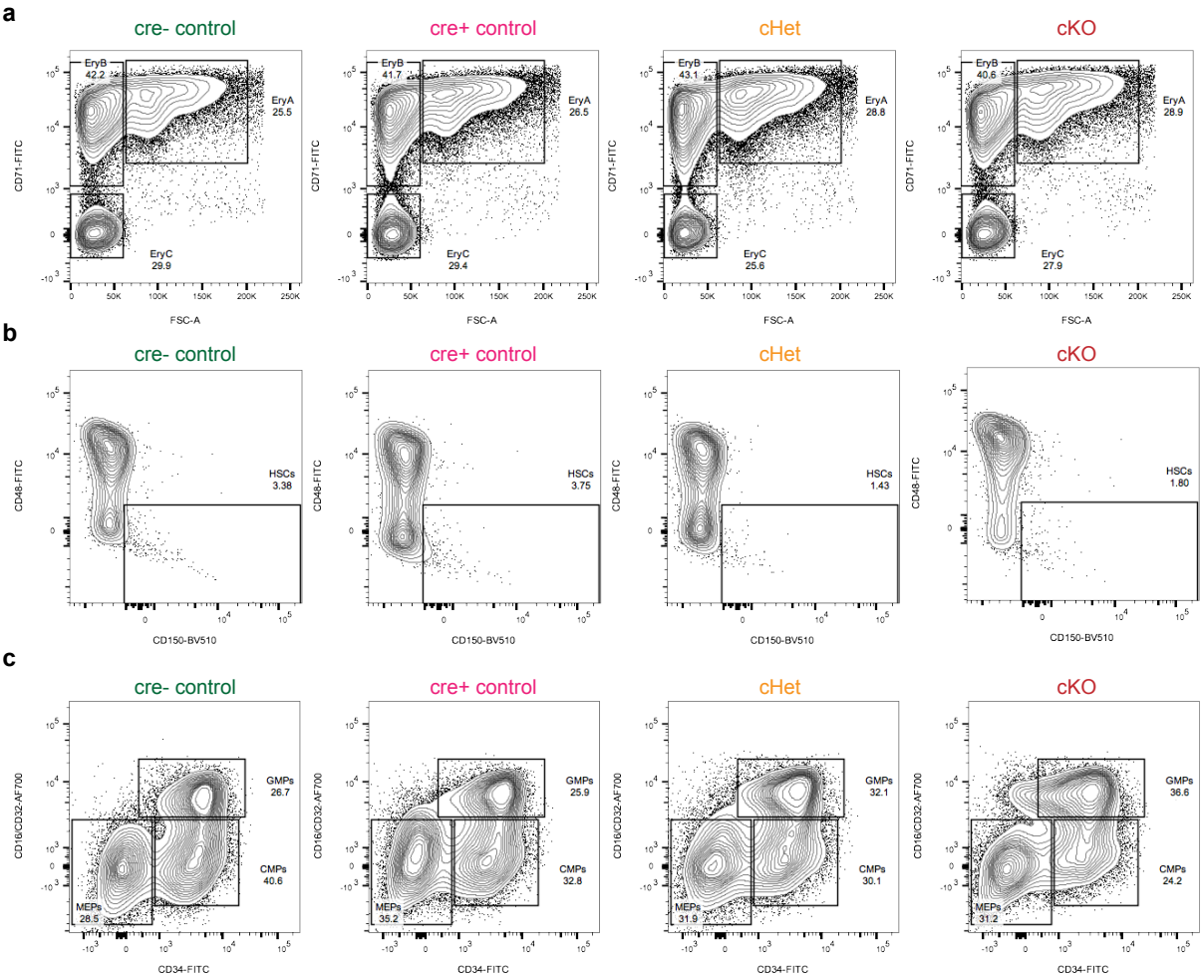

Supplemental Figure 8. Strategy to quantify hematopoietic stem and progenitor cell subsets in hematopoietic-specific *Gdf11* conditional knockout mice. (a-c), Representative flow cytometry analyses of hematopoietic stem and progenitor cell subsets within cre- control, cre+ control, cHet and cKO mice. (a), Erythroid precursor cells (EryA: $CD71^{+}FSC^{high}$; EryB: $CD71^{+}FSC^{low}$; EryC: $CD71^{-}FSC^{low}$). Cells previously gated on live ($7\text{-}AAD^{-}$), $Ter\text{-}119^{+}$ cells. (b), Hematopoietic stem cells (HSCs: $CD48^{-}CD150^{+}$). Cells previously gated on live ($7\text{-}AAD^{-}$), $Lineage^{-}Sca\text{-}1^{+}c\text{-}Kit^{+}$ cells. (c), Myeloid progenitor cells (GMPs: $Fc\gamma R^{+}CD34^{+}$; CMPs: $Fc\gamma R^{low}CD34^{+}$; MEPs: $Fc\gamma R^{-}CD34^{-}$). Cells previously gated on live ($Zombie\ Aqua^{-}$), $Lineage^{-}Sca\text{-}1^{-}c\text{-}Kit^{+}$ cells. CD16/CD32 detects $Fc\gamma R$.

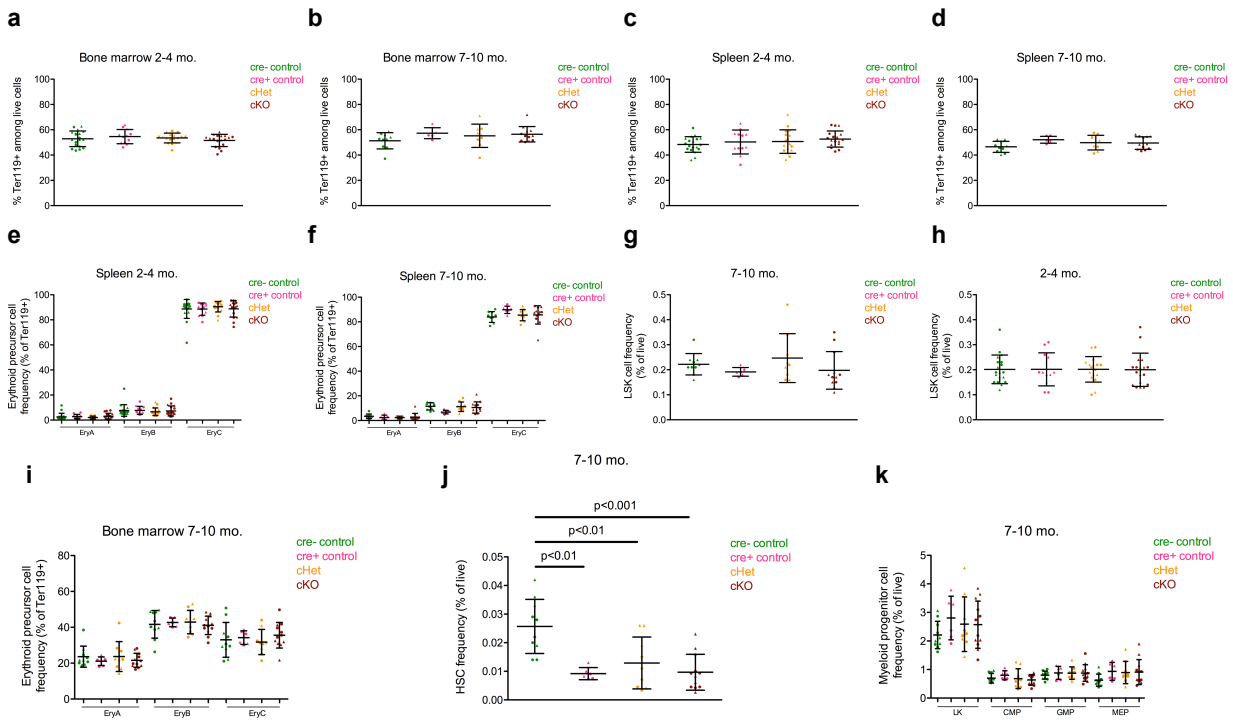

Supplemental Figure 9. Hematopoietic-specific deletion of *Gdf11* does not alter the frequency of Ter-119$^+$ cells or hematopoietic stem and progenitor cells during young adulthood or middle age. (a-d), Frequency of Ter-119$^+$ cells in the (a-b) bone marrow or (c-d) spleen at (a,c) 2-4 months old or (b,d) 7-10 months old (n=6-24 mice per genotype; males and females pooled). (e-f), Frequency of erythroid precursor cells in the spleen of cKO, cHet, cre- control and cre+ control mice (n=6-12 mice per genotype; males and females pooled) at (e) 2-4 months old or (f) 7-10 months old. (g-h), Frequency of Lineage$^-$Sca-1$^+$c-Kit$^+$ cells within the bone marrow of (g) 2-4 month old or (h) 7-10 month old mice. (i-k), Frequency of (i) erythroid precursor cell subsets, (j) hematopoietic stem cells and (k) myeloid progenitor cells within the bone marrow of 7-10 month old mice. Individual data points are overlaid with mean ± SD. Statistics were calculated using a one-way ANOVA with Bonferroni post-test correction, and differences with $p<0.05$ are indicated. Circles: males. Triangles: females.

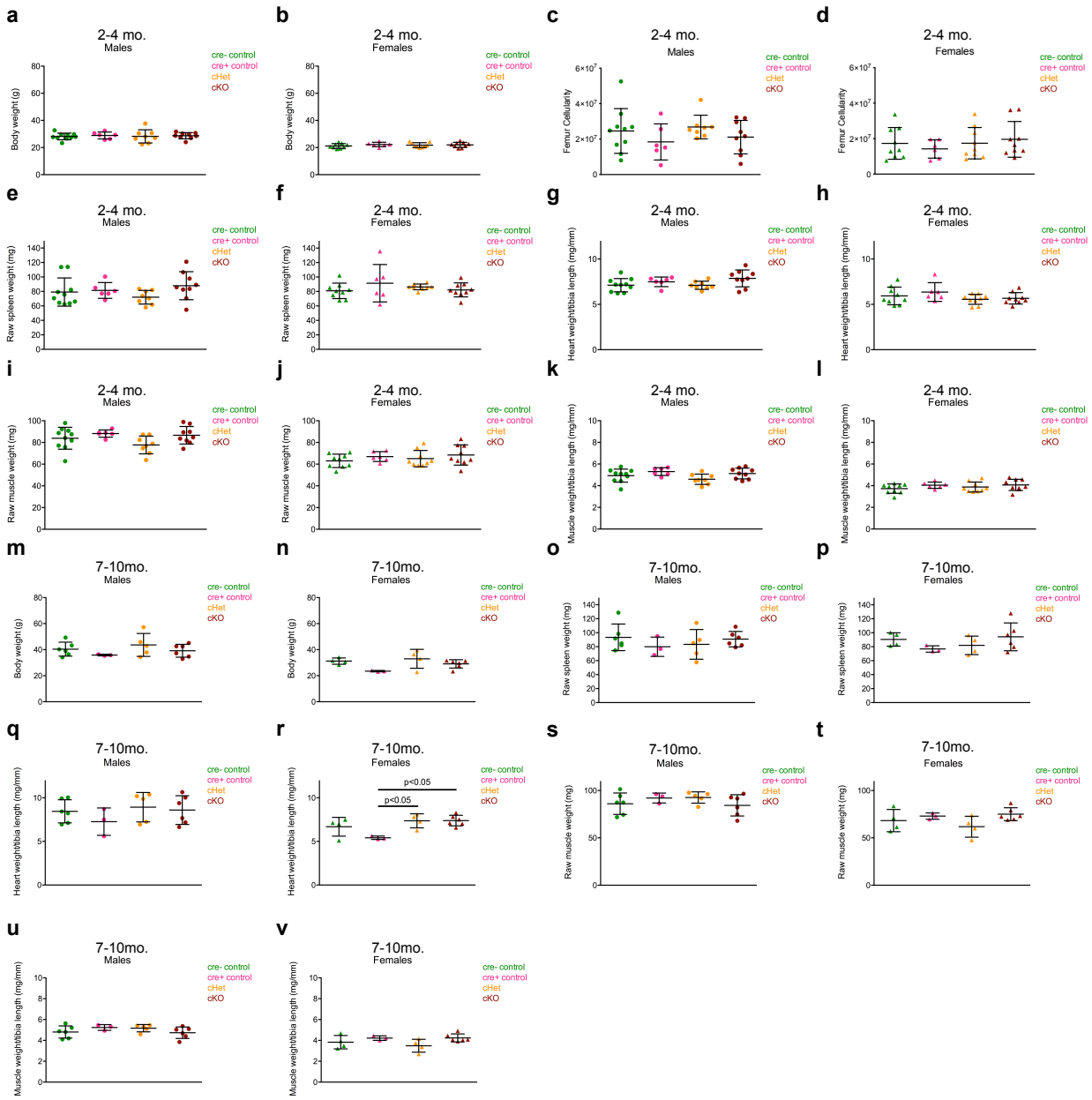

Supplemental Figure 10. Hematopoietic-specific deletion of *Gdf11* does not affect body parameters during young adulthood or middle age. (a-b), Body weight, (c-d), femur cellularity, (e-f), raw spleen weight, (g-h), heart weight/tibia length ratio, (i-j), raw tibialis anterior muscle weight, and (k-l) tibialis anterior muscle weight/tibia length ratio in 2-4 month old mice (n=6-10 mice per sex per genotype). (m-n), Body weight, (o-p), raw spleen weight, (q-r), heart weight/tibia length ratio, (s-t), raw tibialis anterior muscle weight, and (u-v) tibialis anterior muscle weight/tibia length ratio in 7-10 month old mice. (n=3-6 mice per sex per genotype). Individual data points are overlaid with mean ± SD. Statistics were calculated using a one-way ANOVA with Bonferroni post-test correction, and differences with $p<0.05$ are indicated. Circles: males. Triangles: females.

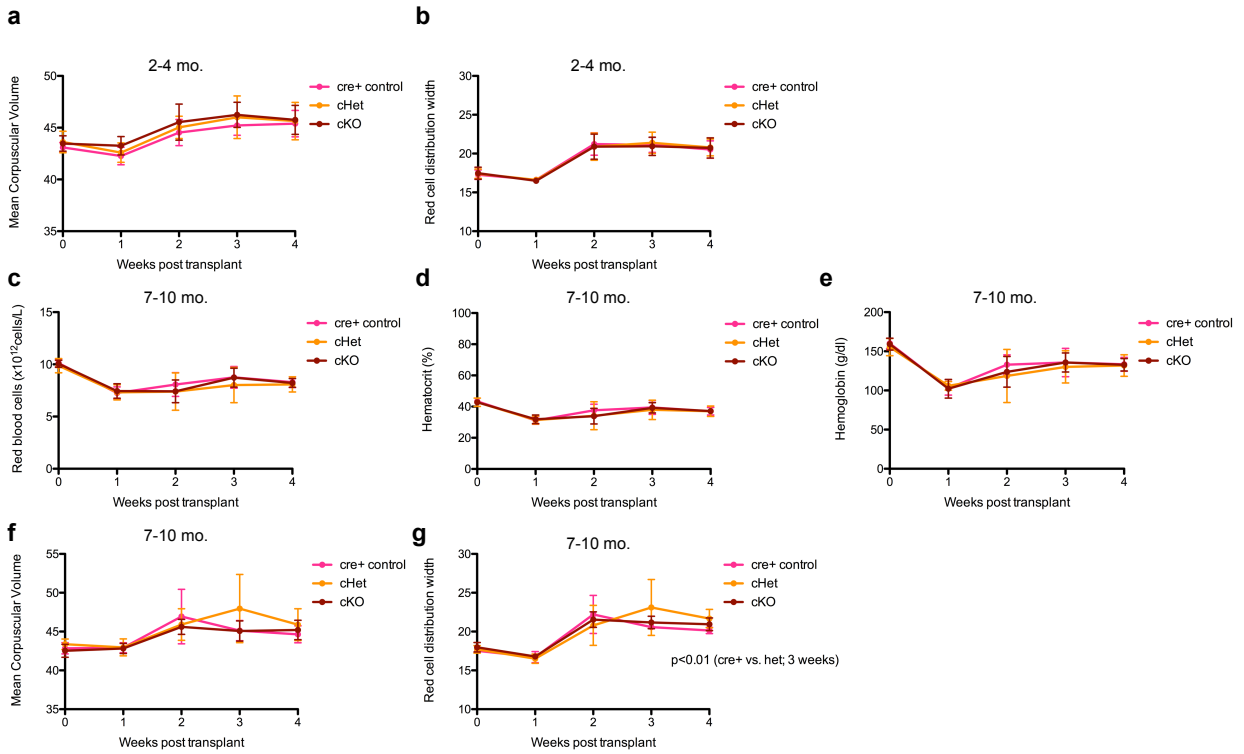

Supplemental Figure 11. Hematopoietic-specific *Gdf11* deletion does not alter red blood cell recovery following bone marrow transplantation. (a-b), (a) Mean corpuscular volume and (b) red cell distribution width in C57BL/6J recipient mice transplanted with cKO, cHet or cre+ control bone marrow cells from 2-4 month old donors. Recipients analyzed at 0, 1, 2, 3 and 4 weeks post-transplant (n=18-20 mice per genotype; males and females pooled). (c), Red blood cell number, (d), hematocrit, (e), hemoglobin levels, (f), mean corpuscular volume and (g), red cell distribution width in C57BL/6J recipient mice transplanted with cKO, cHet or cre+ control bone marrow cells from 7-10 month old donors (n=10-12 mice per genotype; males and females pooled). Data are mean ± SD. Statistics were calculated using a repeated measures ANOVA, and the single difference with $p<0.05$ is indicated.

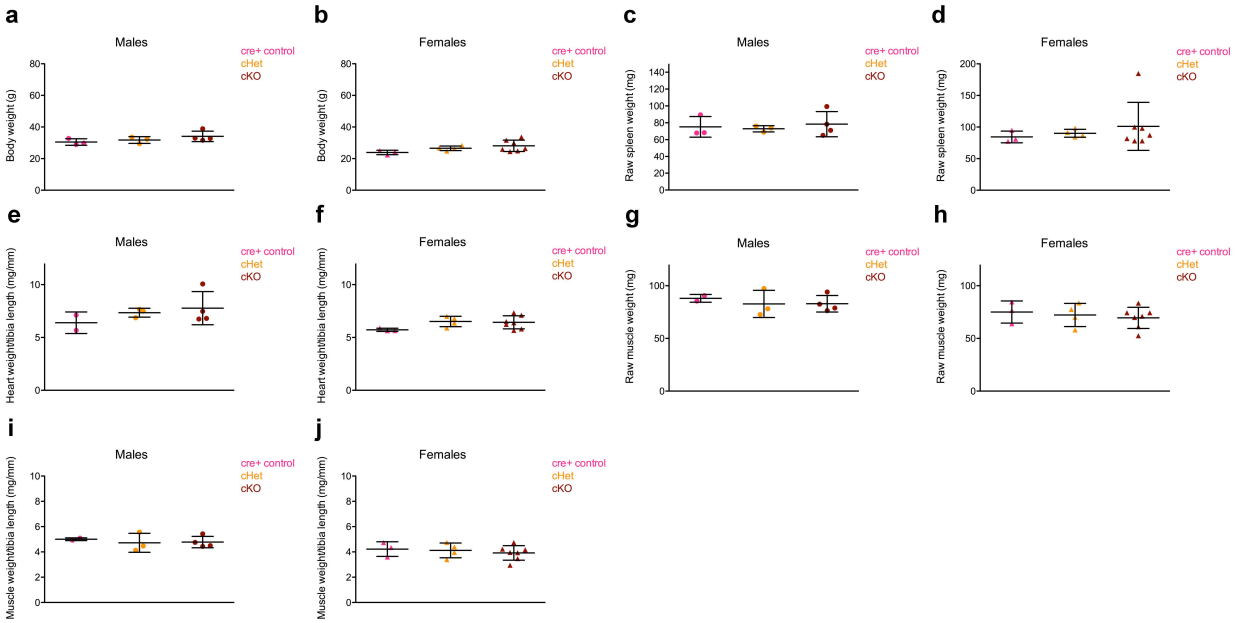

Supplemental Figure 12. Hematopoietic-specific deletion of *Gdf11* does not affect body parameters following bone marrow transplantation. (a-b), Body weight, (c-d), raw spleen weight, (e-f), heart weight/tibia length ratios, (g-h), raw tibialis anterior muscle weight and (i-j), tibialis anterior muscle weight/tibia length ratio in C57BL/6J recipient mice transplanted with cKO, cHet or cre+ control bone marrow cells from 2-4 month old donors (n=2-7 mice per sex per genotype). Individual data points are overlaid with mean ± SD. Statistics were calculated using a one-way ANOVA with Bonferroni post-test correction, and no differences with $p<0.05$ were detected. Circles: males. Triangles: females.

Supplemental References

1. de Boer, J.*, et al.* Transgenic mice with hematopoietic and lymphoid specific expression of Cre. *Eur J Immunol* **33**, 314-325 (2003).
2. Madisen, L.*, et al.* A robust and high-throughput Cre reporting and characterization system for the whole mouse brain. *Nat Neurosci* **13**, 133-140 (2010).
3. McPherron, A.C., Lawler, A.M. & Lee, S.J. Regulation of anterior/posterior patterning of the axial skeleton by growth/differentiation factor 11. *Nat Genet* **22**, 260-264 (1999).
4. McPherron, A.C., Huynh, T.V. & Lee, S.J. Redundancy of myostatin and growth/differentiation factor 11 function. *BMC Dev Biol* **9**, 24 (2009).
5. El-Brolosy, M.A.*, et al.* Genetic compensation triggered by mutant mRNA degradation. *Nature* **568**, 193-197 (2019).
6. Ma, Z.*, et al.* PTC-bearing mRNA elicits a genetic compensation response via Upf3a and COMPASS components. *Nature* **568**, 259-263 (2019).
7. Ruckle, J.*, et al.* Single-dose, randomized, double-blind, placebo-controlled study of ACE-011 (ActRIIA-IgG1) in postmenopausal women. *J Bone Miner Res* **24**, 744-752 (2009).
8. Dussiot, M.*, et al.* An activin receptor IIA ligand trap corrects ineffective erythropoiesis in β-thalassemia. *Nat Med* **20**, 398-407 (2014).
9. Suragani, R.N.*, et al.* Transforming growth factor-β superfamily ligand trap ACE-536 corrects anemia by promoting late-stage erythropoiesis. *Nat Med* **20**, 408-414 (2014).
10. Paulson, R.F. Targeting a new regulator of erythropoiesis to alleviate anemia. *Nat Med* **20**, 334-335 (2014).
11. Katsimpardi, L.*, et al.* Vascular and neurogenic rejuvenation of the aging mouse brain by young systemic factors. *Science* **344**, 630-634 (2014).
12. Loffredo, F.S.*, et al.* Growth differentiation factor 11 is a circulating factor that reverses age-related cardiac hypertrophy. *Cell* **153**, 828-839 (2013).
13. Sinha, M.*, et al.* Restoring systemic GDF11 levels reverses age-related dysfunction in mouse skeletal muscle. *Science* **344**, 649-652 (2014).
14. Poggioli, T.*, et al.* Circulating Growth Differentiation Factor 11/8 Levels Decline With Age. *Circ Res* **118**, 29-37 (2016).
15. Egerman, M.A.*, et al.* GDF11 Increases with Age and Inhibits Skeletal Muscle Regeneration. *Cell Metab* **22**, 164-174 (2015).
16. Schafer, M.J.*, et al.* Quantification of GDF11 and Myostatin in Human Aging and Cardiovascular Disease. *Cell Metab* **23**, 1207-1215 (2016).
17. Pomplun, D., Florian, S., Schulz, T., Pfeiffer, A.F. & Ristow, M. Alterations of pancreatic beta-cell mass and islet number due to Ins2-controlled expression of Cre recombinase: RIP-Cre revisited; part 2. *Horm Metab Res* **39**, 336-340 (2007).
18. Semprini, S.*, et al.* Cryptic loxP sites in mammalian genomes: genome-wide distribution and relevance for the efficiency of BAC/PAC recombineering techniques. *Nucleic Acids Res* **35**, 1402-1410 (2007).
19. Garbern, J.*, et al.* Analysis of Cre-mediated genetic deletion of Gdf11 in cardiomyocytes of young mice. *Am J Physiol Heart Circ Physiol* (2019).

20. Joseph, C.*, et al.* Deciphering hematopoietic stem cells in their niches: a critical appraisal of genetic models, lineage tracing, and imaging strategies. *Cell Stem Cell* **13**, 520-533 (2013).
21. Siegemund, S., Shepherd, J., Xiao, C. & Sauer, K. hCD2-iCre and Vav-iCre mediated gene recombination patterns in murine hematopoietic cells. *PLoS One* **10**, e0124661 (2015).
22. Ogilvy, S.*, et al.* Promoter elements of vav drive transgene expression in vivo throughout the hematopoietic compartment. *Blood* **94**, 1855-1863 (1999).